Available online at www.sciencedirect.com
SCIENCE DIRECT®
ELSEVIER
Mathematical and Computer Modelling 40 (2004) 519–533
MATHEMATICAL AND COMPUTER MODELLING
www.elsevier.com/locate/mcm

# Fixed-Point Methods for a Semiconductor Quantum Dot Model

TSUNG-MIN HWANG
Department of Mathematics, National Taiwan Normal University
Taipei 116, Taiwan, R.O.C.
min@math.ntnu.edu.tw

WEN-WEI LIN
Department of Mathematics, National Tsing Hua University
Hsinchu 300, Taiwan, R.O.C.
wwlin@am.nthu.edu.tw

JINN-LIANG LIU
Department of Applied Mathematics, National Chiao Tung University
Hsinchu 300, Taiwan, R.O.C.
jinnliu@math.nctu.edu.tw

WEICHUNG WANG*
Department of Applied Mathematics, National University of Kaohsiung
Kaohsiung 811, Taiwan, R.O.C.
wwang@nuk.edu.tw

*(Received May 2003; revised and accepted November 2003)*

**Abstract**—This paper presents various fixed-point methods for computing the ground state energy and its associated wave function of a semiconductor quantum dot model. The discretization of the three-dimensional Schrödinger equation leads to a large-scale cubic matrix polynomial eigenvalue problem for which the desired eigenvalue is embedded in the interior of the spectrum. The cubic problem is reformulated in several forms so that the desired eigenpair becomes a fixed point of the new formulations. Several algorithms are then proposed for solving the fixed-point problem. Numerical results show that the simple fixed-point method with acceleration schemes can be very efficient and stable. © 2004 Elsevier Ltd. All rights reserved.

**Keywords**—Cubic eigenvalue problem, Fixed-point method, Linear Jacobi-Davidson method, Linear successive iterations, 3D Schrödinger equation.

## 1. INTRODUCTION

Semiconductor quantum dots (QDs) are nanoscale structures in which the carriers are confined in all three dimensions (3D). The carriers exhibit wavelike properties and discrete energy states in QDs. They have recently attracted intensive research on exploring their physical phenomena and

*Author to whom all correspondence should be addressed.
The authors are grateful for the anonymous referees' suggestions and comments. This work is partially supported by the National Science Council and the National Center for Theoretical Sciences in Taiwan.

0895-7177/04/$ - see front matter © 2004 Elsevier Ltd. All rights reserved. Typeset by AMS-TEX
doi:10.1016/j.mcm.2003.11.006

practical applications [1]. Methods such as photoluminescence [2] and capacitance-voltage [3] spectroscopy have been used to study QDs' electronic and optical properties. For practical applications, QDs also play an important role in optoelectronic devices such as QD infrared photodetectors [4], QD lasers [5], memory device [6], QD computing systems [7], and light emitting diodes [8].

While QDs have been studied theoretically and experimentally, numerical methods can provide useful simulation results. For example, pseudopotential and first-principal methods [9], adiabatic approximation methods [10], and multi-band envelope function [11] are used to study basic QD physical characteristics. These numerical methods, however, may suffer from excessive computing time-consuming or insufficient accuracy for small size QDs [12]. Besides, little results can be acquired by current computational methods for 3D QDs [13, Section 11.6]. On the other hand, various physical models that are most effective, e.g. the finite hard-wall potential model, cannot be solved analytically. Numerical approximations therefore become an essential tool [12].

In this paper, we are interested in calculating the ground state energy level and the associated wave function of a single electron confined in a cylindrical semiconductor QD material embedded in another cylindrical material. The model assumes the effective one electronic band Hamiltonian, the BenDaniel-Duke boundary conditions [14], and nonparabolic electron effective mass depending on energy and position. This model is proposed in [15] and later used and extended in various works [16–19], and in references therein. At the boundary of the QD, the finite hard-wall 3D confinement potential is induced by real discontinuity of the conduction band.

The three-dimensional Schrödinger equation of the model is discretized by finite difference approximation in cylindrical coordinates. Nonuniform mesh by which more grid points are placed around the heterojunction is adopted for capturing rapid changes in the area. One of the major concerns for the numerical treatment of the model is caused by the band nonparabolicity which results in a cubic type of eigenvalue systems. Effective methods for solving cubic eigenvalue problems arising from such a model are rarely available in the literature. We present here several algorithms for solving the cubic eigenvalue problem based on the framework of fixed-point methods. Numerical results are also given to demonstrate the efficiency and accuracy of the proposed methods.

The main results of this paper are briefly summarized as follows.

- The cubic eigenvalue problem is first reformulated into various forms so that the desired eigenpair of the problem is a fixed point (a zero) of the new formulations.
- A fixed-point method is then proposed to find the desired eigenpair. The linear Jacobi-Davidson (JD) method is used in each fixed-point iteration due to the characteristics of the formulation. Two practical acceleration schemes, namely, an initial eigenvector selection strategy for the JD method and an adaptive convergence scheme, are given to improve the convergence performance of the fixed-point method.
- A hybrid method that combines the fixed-point (global and linear) iteration with a local and quadratic Newton iteration when the iterates are close to the desired solution is presented. Again, the JD method is used for the linear eigenvalue problems associated with both fixed point and Newton's iterations.
- Our numerical results indicate that the acceleration schemes can significantly improve the fixed-point method. The hybrid method is slightly more efficient than the fixed-point method. Moreover, a comparison of the fixed-point methods with the nonlinear Jacobi-Davidson (NJD) methods is also given. The NJD methods solve the cubic eigenvalue problem directly and are presented in our earlier paper [20]. We find that the fixed-point methods outperform the NJD in small size ($49,950 \times 49,950$) problems and are comparable to the NJD for middle ($107,055 \times 107,055$) and large ($193,700 \times 193,700$) size problems.

This paper is organized as follows. The model problem and its cubic eigenvalue discrete form are given in Section 2. New formulations of the cubic eigenvalue problem are given in Section 3

for which the fixed-point method and the JD method are then developed. These two methods are first applied to study the convergence behavior with respect to the new formulations from which the best one is thus chosen for further numerical experiments with some acceleration schemes. The hybrid method is given in Section 4. In Section 5, numerical comparison results are presented to illustrate the performance of various combinations of the above methods and schemes. Some concluding remarks are made in Section 6.

## 2. MODEL PROBLEM AND CUBIC EIGENVALUE SYSTEMS

Now we introduce a cylinder hetrostructure semiconductor quantum dot (QD) model that motivates this study. The QD model assumes that a single electron is confined in a QD embedded in the center of another cylindrical matrix material with the same rotational axis. The QD schema is shown in Figure 1. The coordinate of the top of the matrix is denoted by $Z_{\text{mtx}}$. The coordinates of the bottom and the top of the QD are denoted by $Z_{\text{btm}}$ and $Z_{\text{top}}$, respectively. The radii of the dot and matrix are denoted by $R_{\text{dot}}$ and $R_{\text{mtx}}$, respectively.

In the cylindrical coordinates, the QD structure can be described by the 3D time-independent Schrödinger equation

$$\frac{-\hbar^2}{2m_\ell(\lambda)}\left[\frac{\partial^2 F}{\partial r^2}+\frac{1}{r}\frac{\partial F}{\partial r}+\frac{1}{r^2}\frac{\partial^2 F}{\partial \theta^2}+\frac{\partial^2 F}{\partial z^2}\right]+c_\ell F=\lambda F, \tag{1}$$

where $\hbar$ is the Plank constant, $\lambda$ is the total electron energy, and $F = F(r,\theta,z)$ is the wave function. The index $\ell$ depends on $r$ and $z$ and is used to distinguish the region of the quantum dot ($\ell = 1$) from that of the matrix ($\ell = 2$). The notation $m_\ell$ denotes a nonparabolic effective mass approximation depending on energy and position [12,19]. The nonparabolic effective mass is modelled as

$$\frac{1}{m_\ell(\lambda)}=\frac{P_\ell^2}{\hbar^2}\left(\frac{2}{\lambda+g_\ell-c_\ell}+\frac{1}{\lambda+g_\ell-c_\ell+\delta_\ell}\right), \tag{2}$$

where $P_\ell$, $g_\ell$, and $\delta_\ell$ stand for the momentum, main energy gap, and spin-orbit splitting in the $\ell^{\text{th}}$ region, respectively. The Schrödinger equation (1) is equipped with Dirichlet boundary conditions on the top, bottom, and sidewall of the matrix

$$F(r,\theta,Z_{\text{mtx}}) = F(r,\theta,0) = F(R_{\text{mtx}},\theta,z) = 0, \tag{3}$$

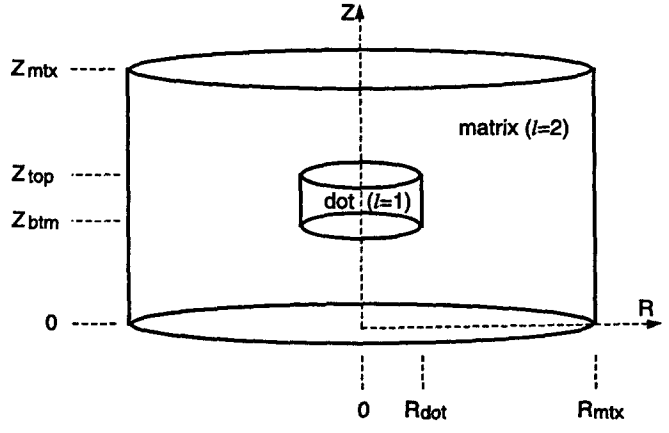


Figure 1. The quantum dot structure schema showing that a cylindrical quantum dot is embedded in a hetrostructure matrix.

and with the BenDaniel-Duke interface conditions [14]

$$\begin{aligned}
\frac{\hbar^2}{m_1(\lambda)}\frac{\partial F}{\partial r}\bigg|_{R_{\text{dot}}^-} &= \frac{\hbar^2}{m_2(\lambda)}\frac{\partial F}{\partial r}\bigg|_{R_{\text{dot}}^+}, \\
\frac{\hbar^2}{2m_2(\lambda)}\frac{\partial F}{\partial z}\bigg|_{Z_{\text{btm}}^-} &= \frac{\hbar^2}{2m_1(\lambda)}\frac{\partial F}{\partial z}\bigg|_{Z_{\text{btm}}^+}, \\
\frac{\hbar^2}{2m_1(\lambda)}\frac{\partial F}{\partial z}\bigg|_{Z_{\text{top}}^-} &= \frac{\hbar^2}{2m_2(\lambda)}\frac{\partial F}{\partial z}\bigg|_{Z_{\text{top}}^+},
\end{aligned} \tag{4}$$

where the + and − signs denote that the corresponding outward normal derivatives on the interface are defined for the matrix and the dot regions, respectively.

To discretize the 3D cylindrical model (1), we choose the mesh points with following two special considerations.

- NONUNIFORM MESH.
  We use uniform mesh lengths in the azimuthal direction. However, since the wave functions change rapidly around the heterojunction (the interfaces), we nonuniformly partition the domain in the radial and axial directions by refining the meshes around the interfaces. Without applying this nonuniform mesh generation scheme, much finer uniform partition over the whole domain would be needed to achieve a similar accuracy compared with that of the nonuniform one. Much more storage and time would then be consumed.
- HALF-SHIFTED MESH WIDTH IN THE RADIAL DIRECTION.
  We modify the two-dimensional disk discretization scheme described in [21] so that the mesh points are shifted with a half mesh width in the radial direction. This setting avoids placing mesh points on the natural axis in the sense that the coefficients of the finite difference functions at the axial axis are cancelled out. Therefore, no pole conditions need to be imposed.

Based on this meshing scheme, we use the standard centered seven-point finite difference to discretize equation (1) and use two-point finite differences to discretize the interface conditions defined in (4). The boundary conditions in (3) are then applied for the numerical boundary values. The discretization results in a large sparse eigenvalue problem with size $\rho\eta\zeta$-by-$\rho\eta\zeta$, where $\rho$, $\eta$, and $\zeta$ denote the mesh point numbers in the radial ($r$), azimuthal ($\theta$), and axial ($z$) direction, respectively. However, by exploiting the periodicity in the azimuth direction and applying suitable permutations and the Fourier transformations, the 3D eigenproblem can be decoupled into $\eta$ independent $\rho\zeta$-by-$\rho\zeta$ 2D eigenproblems as

$$\begin{bmatrix} \tilde{T}_1(\lambda) & & \\ & \ddots & \\ & & \tilde{T}_\eta(\lambda) \end{bmatrix} \begin{bmatrix} \tilde{F}_1 \\ \vdots \\ \tilde{F}_\eta \end{bmatrix} = \begin{bmatrix} \tilde{D}_1(\lambda) & & \\ & \ddots & \\ & & \tilde{D}_\eta(\lambda) \end{bmatrix} \begin{bmatrix} \tilde{F}_1 \\ \vdots \\ \tilde{F}_\eta \end{bmatrix}, \tag{5}$$

where $\tilde{T}_j(\lambda)$ and $\tilde{D}_j(\lambda)$ are $\rho\zeta$-by-$\rho\zeta$ matrices for $j = 1, \ldots, \eta$. Note that all mesh ponints corresponding to a certain $\tilde{F}_j$ have the same $\theta$ value. That is, these mesh points are all located on a certain vertical 2D half-plane. It is worth pointing out that, from the viewpoint of the target quantum dot application, only a 2D eigenproblem associated with $j = 1$ needs to be solved to obtain the smallest positive eigenvalue that is of interest (the ground state energy). These observations dramatically reduce the computational cost without losing accuracy. For more detailed derivation from the 3D system to the 2D subsystems (5), we refer to [20].

Equation (5) leads to $\eta$ independent $\rho\zeta$-by-$\rho\zeta$ subsystems with the form

$$\mathbf{G}(\lambda)\mathbf{F} = \mathbf{D}(\lambda)\mathbf{F}. \tag{6}$$

Note that the entries of the matrix $\mathbf{G}(\lambda)$ involve the eigenvalues $\lambda$ in the denominator originated from the mass equation (2). Multiplying this equation by the common denominator, we obtain the following cubic eigenvalue problem

$$\mathbf{A}(\lambda)\mathbf{F} \equiv \left(\lambda^3 A_3 + \lambda^2 A_2 + \lambda A_1 + A_0\right)\mathbf{F} = 0, \tag{7}$$

where $\lambda \in \mathbb{C}$ is an eigenvalue, $\mathbf{F} \in \mathbb{C}^n$ is an eigenvector, and $A_i$, $i = 0, 1, 2, 3$, are $\lambda$-independent sparse matrices in $\mathbb{R}^{\rho\zeta \times \rho\zeta}$. Our main concern with this problem is to effectively and accurately compute the smallest positive eigenvalue embedded in the interior of the spectrum of (7) together with its associated eigenvector. The detail deduction and full description of the matrices in the eigenproblem (7) are omitted here (see [20] for more details).

It is worth mentioning that the cubic eigenvalue problem (7) can be rewritten as a generalized eigenvalue problem

$$\begin{bmatrix} 0 & I & 0 \\ 0 & 0 & I \\ A_0 & A_1 & A_2 \end{bmatrix} \begin{bmatrix} \mathbf{F} \\ \lambda\mathbf{F} \\ \lambda^2\mathbf{F} \end{bmatrix} = \lambda \begin{bmatrix} I & 0 & 0 \\ 0 & I & 0 \\ 0 & 0 & -A_3 \end{bmatrix} \begin{bmatrix} \mathbf{F} \\ \lambda\mathbf{F} \\ \lambda^2\mathbf{F} \end{bmatrix}. \tag{8}$$

This enlarged linear eigenproblem can then be solved by variations of Lanczos methods, variations of Arnoldi methods, or linear Jacobi-Davidson method [22,23]. Furthermore, well established mathematical theories, numerical methods, and perturbation theories are provided in [24–26]. However, disadvantages of such approach exists. First, the order of the larger matrices are triple and the condition numbers may increase since the set of admissible perturbations for (8) is larger than the set for (7) [27]. Secondly, convergence performance, efficiency, and accuracy may be reduced in solving the enlarged eigenproblem (8). Thirdly, since the interested smallest positive eigenvalues are located in the interior of the spectrum, the shift-and-invert technique should be taken for such a large sparse eigenproblem. But, it costs too much for solving the linear system. Therefore, numerical methods that focus on the original cubic eigenproblem (7) and avoid the obstacles would be helpful. While few methods, such as the quadratic or polynomial Jacobi-Davidson methods [20,28–31], deal with the polynomial eigenproblems, here we propose an alternative fixed-point method for the cubic polynomial eigenproblems.

To provide more characteristic insights about the cubic eigenvalue problem, we show the sparsity patterns of the matrices $A_0$, $A_1$, $A_2$, and $A_3$ for $\rho = 8$ and $\zeta = 12$ in Figure 2. In Figure 3,

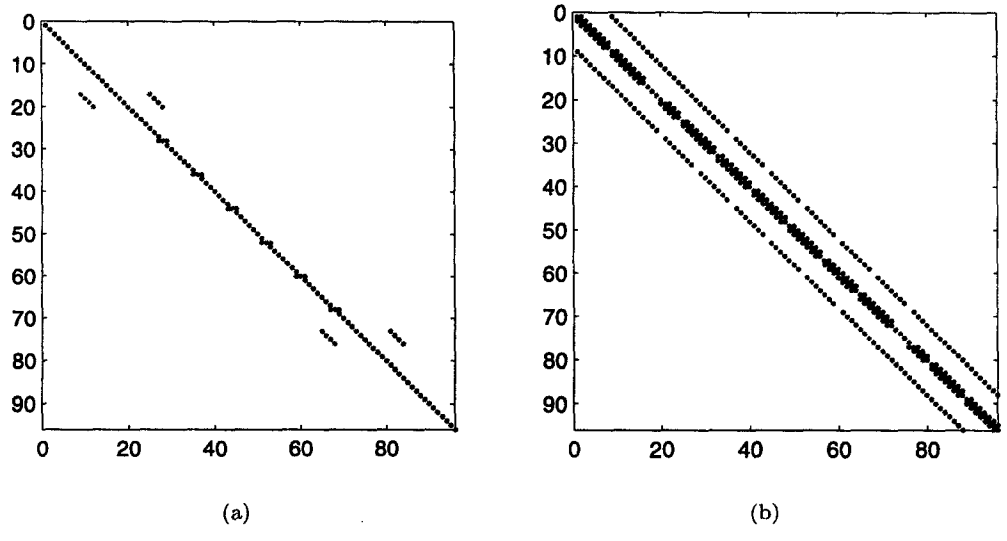


Figure 2. Sparsity patterns of the matrices $A_3$, $A_2$ and $A_1$, $A_0$ are shown in (a) and (b), respectively. The red dots in the figures indicate the components involving interfaces.

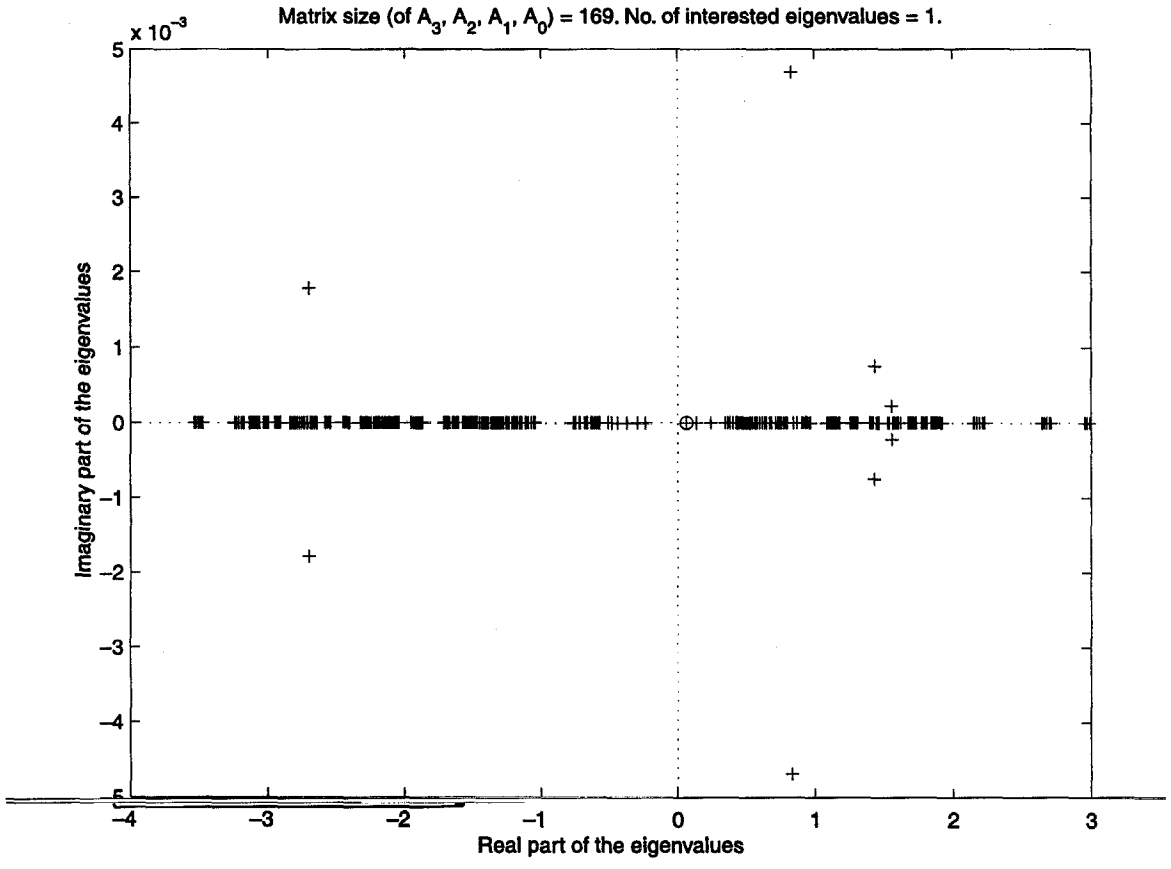


Figure The spectrum of the eigenvalues for a cubic eigenproblem with $A_i \in \mathbb{R}^{169\times 169}$, for $i = 0, 1, 2, 3$. All the computed eigenvalues are plotted by the mark + except the smallest positive eigenvalue (the ground state energy level) by $\oplus$.

we present the spectrum of the eigenvalues of a specific cubic eigenproblem with $A_i \in \mathbb{R}^{169\times 169}$. All the computed eigenvalues are then plotted on the complex plane with the plus marks. The smallest positive eigenvalue (the ground state energy level) is emphasized by the mark $\oplus$. It is clear that the target eigenvalue is embedded in the interior of the eigenvalue spectrum. We now describe our methods for calculating these interior eigenvalues. In what follows, we only consider the first (smallest) eigenpairs. Other eigenpairs can be obtained by some deflation method such as that developed in [32].

While the rational equation (6) and the cubic $\lambda$-matrix polynomial (7) are mathematically equivalent, we consider that the cubic $\lambda$-matrix polynomial (7) is a better formulation from computational viewpoint since by suitably reformulating (7) (see below) the desired eigenvalue can be inverted to the extreme (largest) value of the inverted spectrum whereas the same eigenvalue for (6) is embedded in the interior of the original spectrum. Although the JD method can be used for both formulations, it usually converges faster to the extreme eigenvalues than to the interior ones and thus can benefit from the setting of (7).

## 3. FIXED-POINT AND LINEAR JACOBI-DAVIDSON METHODS

To solve the cubic eigenvalue problem by fixed-point methods, we rewrite equation (7) as

$$\mathbf{A}_d(\lambda)\mathbf{F} = \mu\mathbf{B}_d(\lambda)\mathbf{F}, \qquad d = 1, 2, 3, \tag{9}$$

where $\mu = \lambda^{-d}$ and the matrices $\mathbf{A}_d(\lambda)$ and $\mathbf{B}_d(\lambda)$ are chosen as that shown in Table 1. Although other forms that are equivalent to (9) exist, they did not lead to better performance in our numerical experiments. Consequently, we shall only consider the forms given in the table.

Table 1. Possible choices of $\mathbf{A}_d$ and $\mathbf{B}_d$.

| | $\mathbf{A}_d(\lambda)$ | $\mathbf{B}_d(\lambda)$ | $\mu$ |
|---|---|---|---|
| $d=1$ | $-(\lambda^2 A_3 + \lambda A_2 + A_1)$ | $A_0$ | $1/\lambda$ |
| $d=2$ | $-(\lambda A_3 + A_2)$ | $\lambda A_1 + A_0$ | $1/\lambda^2$ |
| $d=3$ | $-A_3$ | $\lambda^2 A_2 + \lambda A_1 + A_0$ | $1/\lambda^3$ |

We first propose a fixed-point method in Algorithm 1 for solving the cubic eigenvalue problem (7). This algorithm consists of a fixed-point (*outer*) iteration (i.e., in Step (II)) and an *inner* iteration within the linear JD method (i.e., in Step (II.1)) which is given Algorithm 2.

To solve the correction equation approximately in Step (3.5) of Algorithm 2, we compute

$$t \approx -M_{\mathbf{A}}^{-1} r + \varepsilon M_{\mathbf{A}}^{-1} p, \tag{10}$$

where $M_{\mathbf{A}} \approx \mathbf{A}(\theta)$ and $\varepsilon = u^* M_{\mathbf{A}}^{-1} r / u^* M_{\mathbf{A}}^{-1} p$ as suggested in [23]. We further let $M_{\mathbf{A}}$ be the matrix associated with the SSOR preconditioning scheme [33]. Let $\mathbf{A}(\theta) = D - L - U$, where $D$ is the main diagonal of $\mathbf{A}(\theta)$, $L$ and $U$ are the strictly lower and upper triangular matrix of $\mathbf{A}(\theta)$, respectively. The preconditioner $M_{\mathbf{A}} = (D - \omega L) D^{-1} (D - \omega U)$, and $\omega \in (0, 2)$.

ALGORITHM 1. FIXED-POINT METHODS FOR CUBIC EIGENPROBLEMS.

(I) Choose $d = 1, 2$, or 3. Choose $\lambda_i$. Let $i = 0$.

(II) Until ($\lambda_i$ converges to the desired eigenvalue) do

(II.1) Solve $\mathbf{A}_d(\lambda_i)\mathbf{F} = \mu \mathbf{B}_d(\lambda_i)\mathbf{F}$ for $(\mu_{\max}, \mathbf{F}_{\max})$ by linear Jacobi-Davidson method, where $\mu_{\max}$ is the maximum positive eigenvalue and $\mathbf{F}_{\max}$ is the associated eigenvector.

(II.2) Update $i = i + 1$; $\lambda_i = (\mu_{\max})^{-1/d}$.

(III) Output $\lambda_i$ and $\mathbf{F} = \mathbf{F}_{\max}$.

ALGORITHM 2. JACOBI-DAVIDSON METHOD FOR LINEAR EIGENPROBLEM.

(1) Choose an $n$-by-$m$ orthonormal matrix $V$

(2) For $i = 0, 1$

Compute $W_i = A_i V$ and $M_i = V^* W_i$

Endfor

(3) Iterateuntilconvergence

(3.1) Compute the eigenpairs $(\theta, s)$ of $(\theta M_1 + M_0)s = 0$

(3.2) Select the desired (target) eigenpair $(\theta, s)$ with $\| s \|_2 = 1$.

(3.3) Compute $u = Vs$, $p = \mathbf{A}'(\theta)u$, $r = \mathbf{A}(\theta)u$.

(3.4) If ($\|r\|_2 < \varepsilon$), $\lambda = \theta$, $x = u$, Stop

(3.5) Solve (approximately) a $t \perp u$ from $\left(I - \frac{pu^*}{u^* p}\right) \mathbf{A}(\theta)(I - uu^*)t = -r$.

(3.6) Orthogonalize $t$ against $V$, $v = t/\|t\|_2$.

(3.7) For $i = 0, 1$

Compute $w_i = A_i v$

$$M_i = \begin{bmatrix} M_i & V^* w_i \\ v^* W_i & v^* w_i \end{bmatrix}, \quad W_i = [W_i, w_i]$$

Endfor

(3.8) Expand $V = [V, v]$

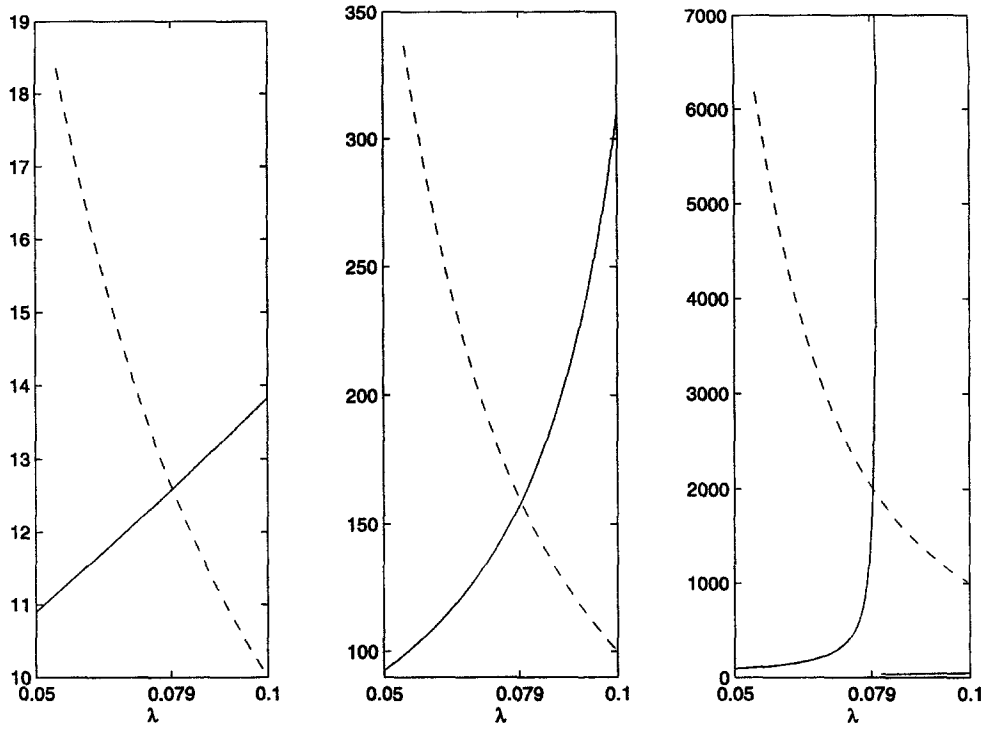


(a) (b) (c)

Figure 4. The eigenvalue curves $y = \mu_{\max}(\lambda)$ (solid lines) and the curves of $y = \lambda^{-d}$ (dash lines) for $d = 1$, 2, 3 are plotted in Part (a), (b), (c), respectively. For $\lambda = 0.0789$, the slope ratio of the tangent lines in absolute value are 0.37, 0.94, and 17, respectively.

To obtain some insights in what convergence behavior we may expect from the fixed-point method of Algorithm 1 for different formulations (i.e., different $d$s) of (9), we first compute the eigenvalue curves $y = \mu_{\max}(\lambda)$ of equation (9) for $\lambda \in [0.05, 0.1]$ with a characteristic selection of the matrices $\mathbf{A}_d$ and $\mathbf{B}_d$ with the matrix size being 1,190. The computed eigencurves (solid lines) are shown in Figure 4 together with the graphics of $y = \lambda^{-d}$ (dash lines) for $d = 1, 2, 3$. These two lines intersect at a certain point with $\lambda = 0.079$ which is also a fixed point of (9). Let $s_1$ and $s_2$ be the slopes of the tangent lines of $y = \lambda^{-d}$ and $y = \mu_{\max}(\lambda)$ at the intersection point, respectively. Then the fixed-point iteration converges provided $|s_2/s_1| < 1$. As shown in Figure 4, the ratio $|s_2/s_1|$ equals to 0.37, 0.94, and 17 for $d = 1, 2, 3$ respectively. In other words, the fixed-point iteration is expected to converge for $d = 1$ and to converge very slowly for $d = 2$ since the ratio is close to 1. Consequently, the formulation ($d = 1$)

$$-(\lambda^2 A_3 + \lambda A_2 + A_1)\mathbf{F} = \frac{1}{\lambda} A_0 \mathbf{F} \tag{11}$$

is the most effective formulation of the model problem (1) when solved by Algorithm 1, and hence, will be used for further numerical experiments hereafter.

Following remark further suggests a theoretically convergence theory regarding the fixed-point scheme. Generally, the scheme iterates the equation

$$\mathbf{A}(\lambda)\mathbf{F}(\lambda) = \frac{1}{\bar{\lambda}(\lambda)} \mathbf{B}(\lambda)\mathbf{F}(\lambda) \tag{12}$$

by giving a $\lambda$, computing the eigenpair $(\mu_{\max}, \mathbf{F}(\lambda))$, and then updating $\lambda = \bar{\lambda}^{1/d} = (1/\mu_{\max})^{1/d} > 0$. We first take the derivative with respect to $\lambda$ of equation (12) to obtain

$$\mathbf{A}'(\lambda)x(\lambda) + \mathbf{A}(\lambda)x'(\lambda) = \frac{-\bar{\lambda}'}{\bar{\lambda}^2} \mathbf{B}(\lambda)x(\lambda) + \frac{1}{\bar{\lambda}} \mathbf{B}'(\lambda)x(\lambda) + \frac{1}{\bar{\lambda}} \mathbf{B}(\lambda)x'(\lambda) \tag{13}$$

Since there exist a left eigenvector $\mathbf{y}(\lambda)$ satisfying

$$\mathbf{y}^\top(\lambda)\mathbf{B}(\lambda)\mathbf{x}(\lambda) = 1 \qquad \text{and} \qquad \mathbf{y}^\top(\lambda)\mathbf{A}(\lambda) = \frac{1}{\bar{\lambda}}\mathbf{y}^\top(\lambda)\mathbf{B}(\lambda) \tag{14}$$

with $\|\mathbf{x}(\lambda)\|_2 = 1$, we multiply $\mathbf{y}^\top$ on the both sides of (13) to obtain

$$\mathbf{y}^\top(\lambda)\mathbf{A}'(\lambda)x(\lambda) + \mathbf{y}^\top(\lambda)\mathbf{A}(\lambda)x\prime(\lambda) = \frac{-\bar{\lambda}'(\lambda)}{\bar{\lambda}^2(\lambda)} + \frac{1}{\bar{\lambda}(\lambda)}\mathbf{y}^\top(\lambda)\mathbf{B}'(\lambda)x(\lambda) + \frac{1}{\bar{\lambda}(\lambda)}\mathbf{y}^\top(\lambda)\mathbf{B}(\lambda)x'(\lambda),$$

or

$$\bar{\lambda}'(\lambda) = -\bar{\lambda}^2(\lambda)\mathbf{y}^\top(\lambda)\mathbf{A}'(\lambda)x(\lambda) + \bar{\lambda}(\lambda)\mathbf{y}^\top(\lambda)\mathbf{B}'(\lambda)x(\lambda). \tag{15}$$

Let the fixed-point mapping be written as

$$\lambda_{k+1} = \left(\bar{\lambda}(\lambda_k)\right)^{1/d},$$

the fixed-point scheme converges locally provided

$$\left|\frac{1}{d}\left(\bar{\lambda}\left(\lambda^*\right)\right)^{1-1/d}\left(\bar{\lambda}'\left(\lambda^*\right)\right)\right| < 1, \tag{16}$$

where $\lambda^*$ is the fixed point and $\bar{\lambda}'$ is defined in equation (15). In short, for the case $d = 1$ particularly, we have $\mathbf{A}(\lambda) = \lambda^2 A_3 + \lambda A_2 + A_1$ and $\mathbf{B}(\lambda) = -A_0$. The scheme thus converges if

$$\left|\frac{1}{d}\left(\lambda^*\right)^{d-1}\left[\lambda^{*^2} y^\top\left(\lambda^*\right)\left(2\lambda^* A_3 + A_2\right)x\left(\lambda^*\right)\right]\right| < 1,$$

for $\bar{\lambda}(\lambda^*) = (\lambda^*)^d$.

We make some remarks on the choice of the linear JD method [22] for solving (11). Various Lanczos, Arnoldi, and JD methods are well developed for calculating extreme values of a spectrum. However, the JD method is suitable not only for calculating extreme eigenvalues but also for calculating interior ones. The hybrid method presented in the next section requires both types of calculations. Another reason is that the preconditioner in the JD method can be robustly chosen so that the inversion involved in the method is relatively inexpensive. It is also worth mentioning that methods that use QR and QZ algorithms for solving the whole spectrum are not recommended for equation (11), since we are only interested in a single interior eigenvalue. Such methods may result in high computational cost and loss of accuracy especially for large problems.

We can further improve the above algorithms by using the following two practical strategies:

- Strategy 1. Since the approximate eigenvector is iteratively more accurate as outer iterations increase, it is natural to use the previous computed eigenvector as an initial eigenvector for the orthonormal matrix in the JD method.
- Strategy 2. Moreover, we can adaptively relax the convergence criteria for the solution procedure in the inner iteration. In the beginning stage, there is no need to apply strict stopping criteria. As the iterates approaching the solution, higher accuracy requirement becomes necessary. Similar methods that adaptively adjust stopping criteria are analyzed and adopted in solving eigenproblems and linear systems in [34] and [35], respectively.

## 4. NEWTON FIXED-POINT METHODS

For nonlinear eigenvalue problems, it is customary to accelerate the iterations by switching the linear solver to a quadratic one when the approximate solution is sufficiently close the exact solution. We now describe our hybrid method that combines both linear and quadratic solvers.

Let $\lambda^*$ be the solution eigenvalue of $\mathbf{A}(\lambda)$ and $\mu = -(\lambda^* - \lambda)$. Since

$$\mathbf{A}(\lambda^*)\mathbf{F} = 0,$$

we have

$$\mathbf{A}\left(\lambda + (\lambda^* - \lambda)\right)\mathbf{F} = 0,$$

$$\left[\mathbf{A}(\lambda) + \frac{d\mathbf{A}(\lambda)}{d\lambda}(\lambda^* - \lambda) + O((\lambda^* - \lambda)^2)\right]\mathbf{F} = 0,$$

or approximately

$$\mathbf{A}(\lambda)\mathbf{F} \approx \mu\frac{d\mathbf{A}(\lambda)}{d\lambda}\mathbf{F}, \tag{17}$$

where

$$\frac{d\mathbf{A}(\lambda)}{d\lambda} = 3\lambda^2 A_3 + 2\lambda A_2 + A_1.$$

By using equation (17), we obtain a so-called linear successive iterative method that is locally quadratic and involves the correction equation

$$\mathbf{A}(\lambda_i)\mathbf{F} = \mu\left(\frac{d\mathbf{A}(\lambda)}{d\lambda}\bigg|_{\lambda=\lambda_i}\right)\mathbf{F}, \tag{18}$$

for an approximate eigenvalue $\lambda_i$. As shown in Algorithm 3, the linearized problem equation (17) is added in Step (II.2.1) and is again solved by the JD method.

ALGORITHM 3. A HYBRID METHOD FOR THE CUBIC EIGENVALUE PROBLEMS.

(I) Choose $d$=1, 2, or 3. Choose $\lambda_i$. Let $i = 0$.
(II) Until ($\lambda_i$ converges to the desired eigenvalue) do
  (II.1) If ($\lambda_i$ is not close to the desired eigenvalue) then
    (II.1.1) Solve $\mathbf{A}_d(\lambda_i)\mathbf{F} = \mu\mathbf{B}_d(\lambda_i)\mathbf{F}$ for $(\mu_{\max}, \mathbf{F}_{\max})$ by linear Jacobi-Davidson method, where $\mu_{\max}$ is the **maximum** positive eigenvalue and $\mathbf{F}_{\max}$ is the associated eigenvector.
    (II.1.2) Update $i = i + 1$, $\lambda_i = (\mu_{\max})^{-d}$, and $\mathbf{F}_i = \mathbf{F}_{\max}$
  (II.2) else
    (II.2.1) Solve $\mathbf{A}(\lambda_i)\mathbf{F} = \mu\left(\frac{d\mathbf{A}(\lambda)}{d\lambda}\Big|_{\lambda=\lambda_i}\right)\mathbf{F}$ for $(\mu_{\min}, \mathbf{F}_{\min})$ by the linear Jacobi-Davidson method, where $\mu_{\min}$ is the **smallest** eigenvalue in absolute value and $\mathbf{F}_{\min}$ is the associated eigenvector.
    (II.2.2) Update $\lambda_{i+1} = \lambda_i - \mu_{\min}$, $i = i + 1$, and then $\mathbf{F}_i = \mathbf{F}_{\min}$.
  (II.3) endif
(III) Output the eigenpair $\lambda_i$ and $\mathbf{F}_i$.

Comparing Algorithms 1 and 3, we notice the following trade-offs between these two algorithms.

(1) Although the quadratic solver in Step (II.2) will converge faster than the linear solver in Step (II.1), it requires more matrix-vector multiplications in the JD method.
(2) The quadratic solver computes the smallest positive eigenvalue that is embedded in the interior of the spectrum whereas the linear solver computes the largest eigenvalue which is an extreme value of the corresponding spectrum. Most methods including the JD method tend to converge more rapidly when extreme eigenvalues are sought.

## 5. NUMERICAL RESULTS

The above methods and schemes can be combined in various ways. We now present numerical results to illustrate computational features of the proposed algorithms. As a typical example, we consider the model with the diameter and the height of the cylindrical QD dot (matrix) being 10 and 5 nm (80 and 30 nm), respectively. The model problem is discretized to the cubic eigenvalue problems (11) with the matrix size of $11,865 \times 11,865$ for $A_i$, $i = 0, 1, 2, 3$. The semiconductor band structure parameters used in the numerical computations are $c_1 = 0.000$, $g_1 = 0.235$, $\delta_1 = 0.81$, $P_1 = 0.2875$, $c_1 = 0.350$, $g_2 = 1.590$, $\delta_2 = 0.80$, and $P_2 = 0.1993$. All the numerical tests are performed on a Compaq AlphaServer DS20E workstation equipped with 667 MHz CPU, one gigabytes main memory, and Compaq Tru64 UNIX Version 5.0.

The following four schemes are tested to show the numerical performance of the algorithms. Schemes 1, 2, and 3 are compared to illustrate the effectiveness of Strategy 1, choosing the initial eigenvector (CIE), and Strategy 2, using adaptive stopping criteria (ASC), as mentioned before. These strategies are also incorporated in Algorithm 3 to get Scheme 4.

SCHEME 1. (FPM). Algorithm 1 is implemented naively. Our JD method is a modification of the JDQZ package (a Jacobi-Davidson eigenvalue problem solver) [36]. Diagonal preconditioners are used. The package randomly assigns initial vector for each of the eigenproblem in the loop of the algorithm. The procedure is considered to be convergent whenever the residual of equation (11) is less than $1.0 \times 10^{-8}$.

SCHEME 2. (FPM_CIE). Starting from the second iteration in Step (II) of Algorithm 1, the approximate eigenvector obtained from the previous iteration is used as the initial vector of the eigenvalue problem solver (JDQZ). The stopping criteria are the same as those of Scheme 1.

SCHEME 3. (FPM_CIE_ASC). In Schemes 1 and 2, a fixed residual tolerance ($1 \times 10^{-8}$) is used in Step (II.1) of Algorithms 1. This scheme instead relaxes this stopping criteria and changes it adaptively according to the following heuristics

$$\texttt{ljd\_tol} = \begin{cases} 1.0 \times 10^{-1}, & \text{if } \texttt{outer\_ite} = 1, \\ \min\left(5.0 \times 10^{-2}, \texttt{residual} \times 0.5\right), & \text{if } \texttt{outer\_ite} \geq 2, \end{cases}$$

where `ljd_tol` is the stopping criterion of the linear Jacobi-Davidson solver, `residual` is the residual of the eigenvalue problem solved in the previous iteration, and `outer_ite` is the iteration number of the loop in Step (II) of Algorithm 1. Similar to Scheme 2, this scheme uses the previous approximate eigenvector as the initial guess for the current linear eigenvalue problem.

SCHEME 4. (FP_LS_CIE_ASC). This scheme switches to the quadratic solver whenever the residual of equation (11) is less than $1.0 \times 10^{-4}$. The previous outer iteration approximate eigenvector is again used as the initial guess for both linear and quadratic inner iterations. The ASC strategy is applied to the linear solver while the fixed stopping criterion ($1 \times 10^{-8}$) is used in the quadratic solver.

In all tests, all the schemes successfully converge to the first eigenpair within the error tolerance. Numerical results are summarized in Figure 5 in which Part (a) shows the numbers of inner and outer iterations with respect to each one of the above four schemes, Part (b) illustrates their convergence behavior in term of error residuals and outer iteration numbers, and Part (c) gives the timing results. By observing this figure, we make the following remarks on the proposed algorithms.

The first part of the numerical results indicates the performance of the fixed-point method (Algorithm 1, $d = 1$).

- As shown in Part (a), Scheme 1 takes about 42–70 inner iterations to converge. By using the approximated eigenvectors as the initial vectors, Scheme 2 converges much faster with the same stopping criteria. From the fifth outer iteration on, the iteration number is

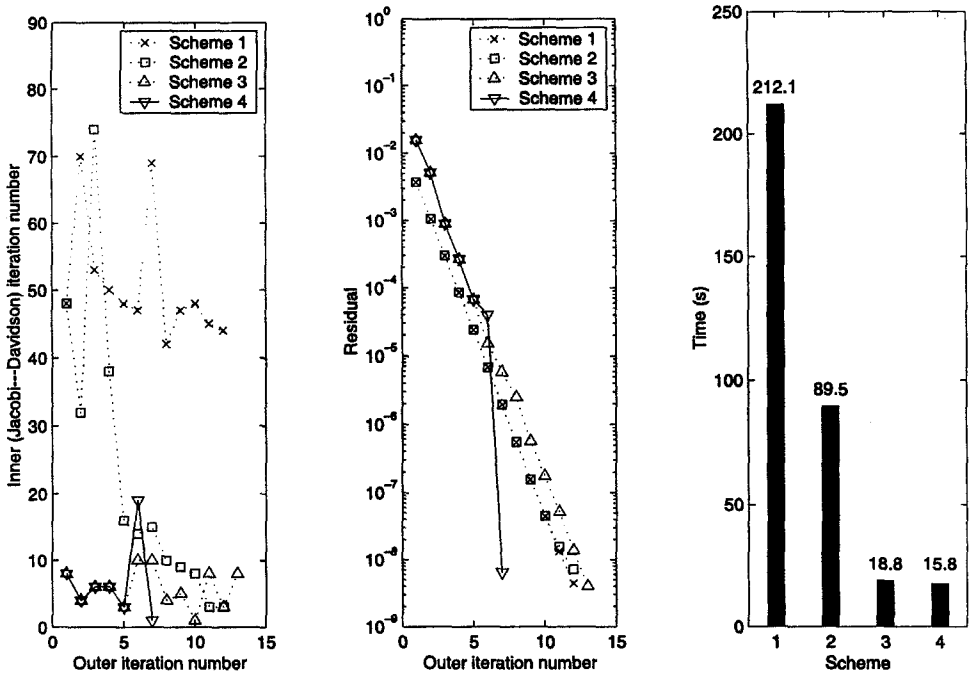


Figure 5. Computational and comparison results of Schemes 1, 2, 3, and 4.

less than 20. By further applying the adaptive stopping criteria in Scheme 3, the inner iteration number dramatically drops below 10 for all cases of outer iterations.

- In terms of error residuals, Schemes 1, 2, and 3 have similar convergence behavior as shown in Part (b).
- In terms of timing, Scheme 3 greatly outperforms the other two schemes. It took about 19 seconds in comparison with 212 and 90 seconds for Schemes 1 and 2, respectively. The saving is about 90% when compared with Scheme 1.

The second part is a comparison between Schemes 3 and 4.

- For Scheme 4, the inner iteration numbers are all less than 10, except for the sixth outer iteration. This is because the tolerance in the sixth (and thereafter) outer iteration is $1 \times 10^{-8}$, about 4 order smaller than the tolerance of the fifth outer iteration. Note that if we use the adaptive stopping criteria (ASC) in the quadratic solver, then these two schemes will behave in a similar way.
- Scheme 4 requires much less outer iterations in terms of error residuals as shown in Part (b). Moreover, it indeed exhibits a quadratic convergence after the sixth iteration when it switches to the quadratic solver.
- Scheme 4 is slightly better than Scheme 3 in terms of timing as shown in Part (c).

In summary, Strategies 1 and 2 significantly improve the efficiency of the fixed-point method without downgrading the overall stability and accuracy. Although Scheme 3 is slightly slower than Scheme 4, it is easier to implement since no additional (quadratic) solver is involved.

A final remark compares the performance of the fixed-point methods (FPM_CIE_ASC and FP_LS_CIE_ASC) with the implementation based on the nonlinear Jacobi-Davidson method proposed in [20, Algorithm 4]. The numerical results are shown in Figure 6. The size of the three tested problems are 49,950 (Parts (a) and (b)), 107,055 (Parts (c) and (d)), and 193,700 (Parts (e) and (f)) for $A_i$, $i = 0, 1, 2, 3$. The parameters $\omega$ in the SSOR preconditioner are equal to 0.1, 0.2, ..., 1.9. The results associated with ground state energy ($j = 1$ in equation (5)) and an excited state energy ($j = 2$ in equation (5)) are shown in the left column (Parts (a), (c), (e)) and

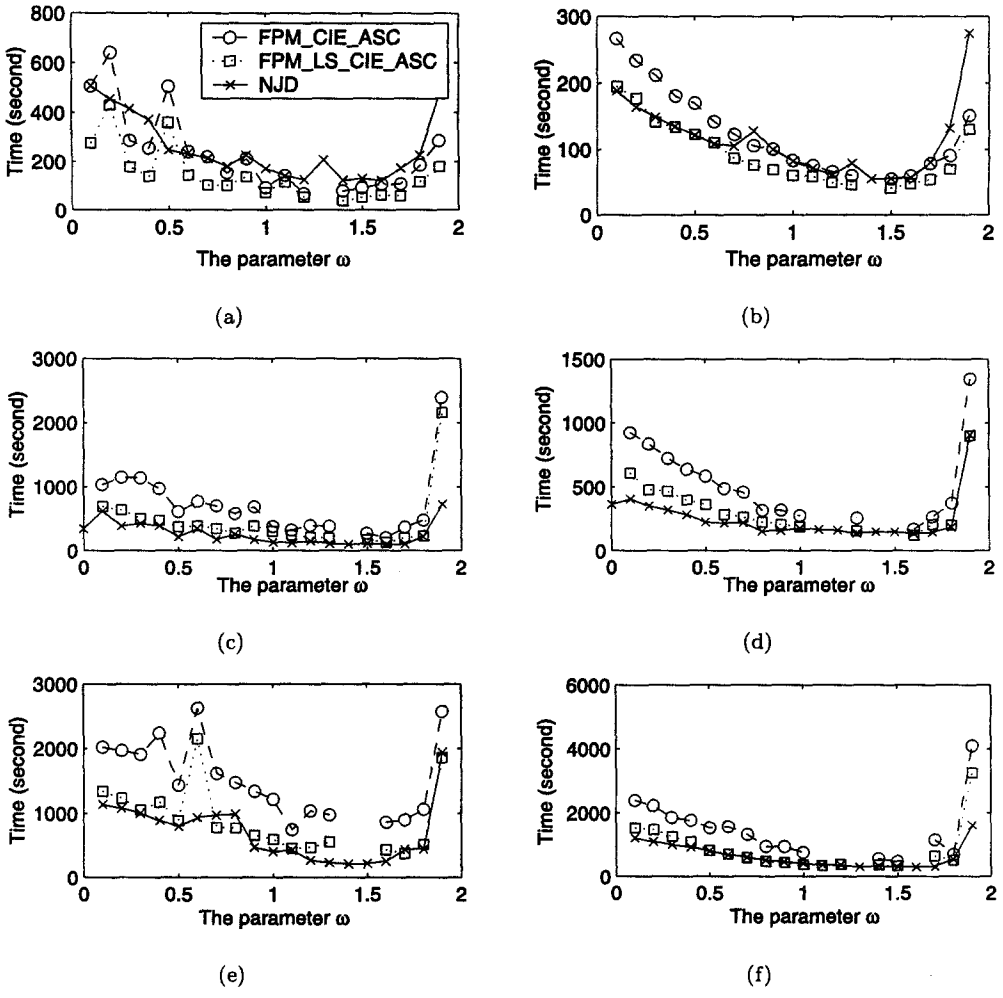


Figure 6. Numerical comparisons of the fixed-point methods (FPM_CIE_ASC and FP_LS_CIE_ASC) and the nonlinear Jacobi-Davidson method. Parts (a) and (b), (c) and (d), and (e) and (f) are associated with a small ($A_i \in \mathbb{R}^{49,950\times 49,950}$), a middle ($A_i \in \mathbb{R}^{107,055\times 107,055}$), and a large ($A_i \in \mathbb{R}^{193,700\times 193,700}$) problem, respectively. The results associated with ground state energy ($j = 1$ in equation (5)) and an excited state energy ($j = 2$ in equation (5)) are shown in the left column (Parts (a), (c), (e)) and right column (Parts (b), (d), (f)), respectively.

right column (Parts (b), (d), (f)), respectively. The figure omits the cases that are not converged in a reasonable time. The numerical comparisons suggest that the FP_LS_CIE_ASC method can outperform the nonlinear Jacobi-Davidson method in small problem and can be competitive in the middle and large problems. The nonlinear Jacobi-Davidson method, however, is more stable in the sense that it successfully converge in all $\omega$ cases.

## 6. CONCLUSION

This paper is concerned with efficient and accurate methods for calculating the ground state energy and its associated wave function of a semiconductor quantum dot model. Our main concern for this model is the numerical treatment of the difficulty incurred by the nonparabolic band structure which results in a cubic type of nonlinear eigenvalue problems from a finite difference discretization. These problems are then reformulated in several forms so that the desired eigenpair becomes a fixed point of the new formulations from which the most effective formulation is then chosen for our numerical experiments on the model. To compute the desired eigenpair, a fixed-point method incorporated with the linear Jacobi-Davidson method is proposed

for solving this new form of the cubic eigenvalue problem. Two practical strategies are presented to improve the fixed-point algorithm in a very significant way. Moreover, a hybrid algorithm that combines both linear (fixed-point iteration) and quadratic (Newton's iteration) solvers are also developed to further improve the convergence behavior of the methods. Numerical experiments demonstrate the effectiveness of the fixed-point methods and the efficiency of the acceleration schemes. Computational results suggest that the hybrid method is most efficient in terms of timing and convergence but with a price of more complicated implementation. Furthermore, the fixed-point methods outperform the NJD methods in small problems and are comparable to the NJD methods for larger size problems.

## REFERENCES


1. L. Jacak, P. Hawrylak and A. Wójs, *Quantum Dots*, Springer, Berlin, (1998).
2. R. Heitz, M. Veit, N.N. Ledentsov, A. Hoffmann, D. Bimberg, V.M. Ustinov, P.S. Kopév and Zh.I. Alferov, Energy relaxation by multiphonon processes in InAs/GaAs quantum dots, *Phys. Rev. B* **56**, 10435–10445, (1997).
3. G. Medeiros-Ribeiro, J.M. Garcia and P.M. Petroff, Charging dynamics of InAs self-assembled quantum dots, *Phys. Rev. B* **56**, 3609–3612, (1997).
4. S. Maimon, E. Finkman, G. Bahir, S.E. Schacham, J.M. Garcia and P.M. Petroff, Intersublevel transitions in InAs/GaAs quantum dots infrared photodetectors, *Appl. Phys. Lett.* **73**, 2003–2005, (1998).
5. L. Harris, D.J. Mowbray, M.S. Skolnick, M. Hopkinson and G. Hill, Emission spectra and mode structure of InAs/GaAs self-organized quantum dot lasers, *Appl. Phys. Lett.* **73**, 969–971, (1998).
6. G. Iannaccone, A. Trellakis and U. Ravaioli, Simulation of a quantum-dot flash memory, *Journal of Applied Physics* **84** (9), 5032–5036, (1998).
7. G. Burkard, D. Loss and D.P. DiVincenzo, Couple quantum dots as quantum gates, *Phys.Rev. B* **59**, 2070–2078, (1999).
8. A. Fiore, U. Oesterle, R. Stanley, R. Houdré, F. Lelarge, M. Ilegems, P. Borri, W. Langbein, D. Birkedal, J.M. Hvam, M. Cantoni and F. Bobard, Structural and electrooptical characteristics of quantum dots emitting at 1.3 $\mu$m on gallium arsenide, *IEEE Journal of Quantum Electronics* **37** (8), (2001).
9. A.J. Williamson and A. Zunger, InAs quantum dots: Predicted electronic structure of free-standing versus GaAs-embedded structures, *Phys. Rev. B* **59**, 15819–15824, (1999).
10. F.M. Peeters and V.A. Schweigert, Two-electron quantum disks, *Phys. Rev. B* **53**, 1468–1474, (1996).
11. J. Shumway, L.R.C. Fonseca, J.P. Leburton, R.M. Martin and D.M. Ceperley, Electronic structure of self-assembled quantum dots: comparison between density functional theory and diffusion quantum Monte Carlo, *Physica E* **8**, 260–268, (2000).
12. Y. Li, J.-L. Liu, O. Voskoboynikov, C.P. Lee and S.M. Sze, *Comput. Phys. Commun.* **140**, 399–404, (2001).
13. P. Harrison, *Quantum Wells, Wires, and Dots: Theoretical and Computational Physics*, John Wiley & Sons, (2000).
14. D.J. Ben Daniel and C.B. Duke, Space-charge effects on electron tunnelling, *Phys. Rev.* **152** (683), (1966).
15. E.A. de Andrada e Silva, G.C. La Rocca and F. Bassani, Spin-orbit splitting of electronic states in semiconductor asymmetric quantum wells, *Phys. Rev. B* **55** (24), 16293, (1997).
16. E.A. de Andrada e Silva, Optical transition energies for lead-salt semiconductor quantum wells, *Phys. Rev. B* **60** (12), 8859, (1999).
17. Th. Schapers, G. Engels, J. Lange, Th. Klocke, M. Hollfelder and H. Luth, Effect of the heterointerface on the spin splitting in modulation doped $In_{(x)}Ga_{(1-x)}As/InP$ quantum wells for $b \to 0$, *J. Appl. Physi.* **83** (8), 4324, (1998).
18. O. Voskoboynikov, C.P. Lee and O. Tretyak, Spin-orbit splitting in semiconductor quantum dots with a parabolic confinement potential, *Phys. Rev. B* **63**, 165306, (2001).
19. O. Voskoboynikov, S.S. Liu and C.P. Lee, Spin-dependent electronic tunnelling at zero magnetic field, *Physical Review B* **58** (23), 15397–15400, (December 1998).
20. W. Wang, T.-M. Hwang, W.-W. Lin and J.-L. Liu, Numerical methods for semiconductor heterostructures with band nonparabolicity, *Journal of Computational Physics* **190** (1), 141–158, (2003).
21. M.-C. Lai, A note on finite difference discretizations for Poisson equation on a disk, *Numerical Methods for Partial Differential Equations* **17** (3), 199–203, (2001).
22. Z. Bai, J. Demmel, J. Dongarra, A. Ruhe and H. van der Vorst, *Templates for the Solution of Algebraic Eigenvalue Problems: A Practical Guide*, SIAM, Philadelphia, PA, (2000).
23. G.L.G. Sleijpen and H.A. van der Vorst. The Jacobi-Davidson method for eigenvalue problems and its relation with accelerated inexact Newton schemes, In *Iterative methods in Linear Algebra, II., Volume 3 of IMACS Series in Computational and Applied Mathematics*, Proceedings of the Second IMACS International Symposium on Iterative Methods in Linear Algebra, June 17-20, 1995, Blagoevgrad, (Edited by Svetozar D. Margenov and Panayot S. Vassilevski), pp. 377–389, IMACS, New Brunswick, NJ, (1996).

24. E. Anderson, Z. Bai, C. Bischof, S. Blackford, J. Demmel, J. Dongarra, J. Du Croz, A. Greenbaum, S. Hammarling, A. McKenney and D. Sorensen, *LAPACK Users' Guide*, Third Edition, SIAM, Philadelphia, PA, (1999).
25. G.H. Golub and C.F. Van Loan, *Matrix Computations*, Third Edition, Johns Hopkins University Press, Baltimore, MD, (1996).
26. G.W. Stewart and J.-G. Sun, *Matrix Perturbation Theory*, Academic Press, New York, (1990).
27. F. Tisseur, Backward error analysis of polynomial eigenvalue problems, *Linear Algebra Appl.* **309**, 339–361, (2000).
28. T. Betcke and H. Voss, A Jacobi-Davidson type projection method for nonlinear eigenvalue problems (Preprint), (2002).
29. M.E. Hochstenbach and H.A. van der Vorst, Alternatives to the Rayleigh quotient for the quadratic eigenvalue problem, Technical Report 1212, Department of Mathematics, University of Utrecht, Utrecht, The Netherlands, (2001).
30. G.L.G. Sleijpen, A.G.L. Booten, D.R. Fokkema and H.A. van der Vorst, Jacobi-Davidson type methods for generalized eigenproblems and polynomial eigenproblems, *BIT* **36** (3), 595–633, (1996).
31. G.L.G. Sleijpen, H.A. van der Vorst and M. van Gijzen, Quadratic eigenproblems are no problem, *SIAM News* **29**, 8–9, (1996).
32. J.-S. Guo, W.-W. Lin and C.-S. Wang, Nonequivalence deflation for the solution of matrix latent value problems, *Linear Algebra and Its Applications* **231**, 15–45, (1995).
33. J. Stoer and R. Bulirsch, *Introduction to Numerical Analysis*, Springer Verlag, (2002).
34. Y.-L. Lai, K.Y. Lin and W.-W. Lin, An inexact inverse iteration for large sparse eigenvalue problems, *Num. Lin. Alg. Appl.* **4** (5), 425–437, (1997).
35. W. Wang and D.P. O'Leary, Adaptive use of iterative methods in predictor-corrector interior point methods for linear programming, *Numerical Algorithms* **25**, 387–406, (2000).
36. D.R. Fokkema and M.B. van Gijzen, *Short Manual for the JDQZ-Package*, (July 1999).